Friction

Research Article

Tangential fretting wear of amorphous carbon films: Evolution of fretting regimes and wear mechanisms

Zhaofan Yue[1,2], Xiaoqiang Fan[2,✉], Fanya Jin[1,✉], Yangfang Li[1], Min Dan[1], Hao Li[2], Minhao Zhu[2], Junyan Zhang[3]

Cite this article: Yue ZF, Fan XQ, Jin FY, et al. *Friction* 2026, **14**(11): 9441237. https://doi.org/10.26599/FRICT.2026.9441237

ABSTRACT: While amorphous carbon-based films are recognized for their efficacy in mitigating fretting wear, because tribopairs demonstrate divergent tribological responses under different fretting states, it remains essential to explore their friction-mitigation mechanisms across distinct fretting regimes and elucidate the evolutionary patterns of these regimes. This effort is critical to gaining thorough and systematic insights into the fretting characteristics of amorphous carbon-based films. The running conditions fretting map was constructed via friction force–displacement curves, and the evolutionary relationship between the two fretting regimes was explored. Additionally, the wear mechanisms and friction-mitigation mechanisms under these two regimes were systematically investigated via advanced characterization techniques, including focused ion beam–transmission electron microscopy (FIB-TEM), scanning electron microscope (SEM), Raman spectroscopy, and X-ray photoelectron spectroscopy (XPS). The results show that increasing the normal load shifts the fretting regime toward the partial slip regime, leading to a decreased friction coefficient and increased wear volume, dissipated energy, and tangential stiffness. Increasing displacement amplitude drives the fretting regime to evolve toward the slip regime, resulting in an increased friction coefficient, wear volume, and dissipated energy, along with decreased tangential stiffness. Notably, an amorphous–nanocrystalline composite structure, in which iron oxides are encapsulated by a graphitized carbon film, forms on the surface of counterpart balls in the slip regime. This structure exerts a pivotal effect on mitigating the friction coefficient and fretting wear. Furthermore, this work advances the fundamental understanding of the mechanisms governing the tangential fretting wear of diamond-like carbon (DLC) films and offers valuable design guidance and a robust theoretical basis for alleviating fretting damage.

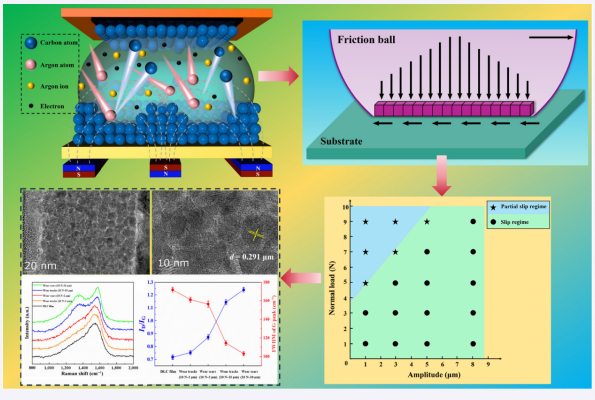

KEYWORDS: fretting wear; fretting regime; amorphous carbon film; transfer film

1 Introduction

Fretting describes ultrasmall amplitude relative motion (typically micrometer-scale) between contacting surfaces subjected to alternating loads, encompassing mechanical vibration, electromagnetic vibration, flow-induced vibration, or thermal cycling [1]. It commonly occurs in interference-fitted mechanical components [2]. Fretting-induced damage to contact surfaces primarily involves wear and fatigue [3]: Fretting wear causes material loss and dimensional changes in components, while fretting fatigue facilitates the initiation and growth of cracks on contact surfaces. Insignificant frictional heating resulting from the ultrasmall displacement amplitude renders fretting highly concealed, posing substantial potential hazards to equipment reliability and safety [4–6].

Fretting has garnered extensive attention across diverse fields, including transportation [7, 8], mechanical engineering [9, 10], and biomedical applications [11–13]. Current research indicates that the optimal strategy to mitigate fretting damage is to deposit solid lubricating films on contact surfaces via surface engineering techniques without modifying the original substrate materials or structural designs [14, 15]. This approach simultaneously reduces or eliminates slip and mixed regimes, enhances contact surface strength, and lowers the friction coefficient, thereby maximizing fretting damage mitigation. While fluid lubricants commonly used to reduce sliding and rolling friction and wear are effective at lowering the friction coefficient, they are not well suited for fretting scenarios [16]. This is primarily because lubricating greases fail to form stable lubricating layers under high vibration frequencies and contact pressures [17], and more critically, fluid lubricants can be squeezed into fretting fatigue-induced cracks, accelerating crack propagation and exacerbating damage [18].

[1] Southwestern Institute of Physics, Chengdu 610207, China. [2] School of Materials Science and Engineering, Southwest Jiaotong University, Chengdu 610031, China. [3] Lanzhou Institute of Chemical Physics, Chinese Academy of Sciences, Lanzhou 730000, China.

✉ Corresponding authors. E-mail: X. Fan, fxq@home.swjtu.edu.cn; F. Jin, yafanjin@163.com

Received: December 1, 2025; Revised: January 7, 2026; Accepted: February 20, 2026

Diamond-like carbon (DLC) is a three-dimensional (3D) network structure formed by a mixture of sp^2-hybridized carbon and sp^3-hybridized carbon, usually presenting an amorphous state or an amorphous–nanocrystalline composite structure [19, 20]. As a solid lubricant film with well-established preparation technology, DLC films deliver exceptional tribological properties coupled with prominent mechanical performance, prominent chemical inertness, and good biocompatibility. Thus, they find applications in diverse fields, including aerospace, rail transit, and bionic medical materials [21–24]. Across the wide range of practical application scenarios, DLC films demonstrate notable suitability for fretting service environments, owing to their distinct structural characteristics.

DLC films have two inherent advantages in fretting wear. First, the small displacement amplitude of fretting makes it difficult to promptly discharge the generated wear debris, which tends to accumulate as a third-body layer between contact surfaces and induce severe abrasive wear on the substrate [25]. However, following the running-in stage, DLC films generate a graphitized transfer layer on the counterpart's surface, which markedly lowers interfacial shear stress, suppresses additional wear, and thereby provides enhanced protection for the substrate [26]. Second, fretting regime regulation can be realized by tuning the film's sp^2/sp^3 hybridization ratio and short-range ordered microstructure, enabling the fabrication of optimal films for specific operating conditions [27]. Drawing on these two properties, investigations into the tribological behavior of DLC coatings in fretting environments have steadily expanded in recent years [28–31].

Nonetheless, most existing research on the fretting properties of DLC films has notable constraints. Compared with sliding and rolling, the most distinctive feature of fretting is the existence of a partial slip regime (PSR). Fretting tribology is essentially the discipline that investigates the tribological characteristics of tribopairs across different fretting regimes and the evolutionary laws governing the transition of these regimes. Thus, studies on the fretting characteristics of materials should not be merely considered as sliding friction characterized by ultrasmall displacement amplitudes. Instead, it is essential to investigate the fretting behavior of materials in different fretting regimes separately by integrating friction force–displacement amplitude curves and examining the evolutionary laws of key parameters such as dissipated energy with varying operating conditions within each regime. In this way, a relatively complete description of the fretting behavior of materials can be provided. Building on the aforementioned considerations, the present study systematically examines the tangential fretting wear performance of DLC films, analyzes the effects of operating conditions on such behavior, establishes and summarizes the running condition fretting map (RCFM), and places particular emphasis on elucidating the evolutionary patterns of the antiwear mechanisms of DLC films across the two fretting regimes.

2 Materials and methods

2.1 Materials

A closed field unbalanced magnetron sputtering system equipped with a graphite target was utilized for the deposition of DLC films onto AISI 304 sheets (Fig. 1). In the fretting experiment, the friction pair consisted of 100Cr6 (GCr15) balls and AISI 304 stainless steel sheets with the DLC film deposited on them. Both the stainless steel sheet (25 mm in diameter, 8 mm in thickness) and the 100Cr6 steel ball (10 mm in diameter) were employed in the experiments. Prior to film deposition, the stainless steel sheets were subjected to ultrasonic cleaning in acetone and alcohol for approximately 20 min. Subsequent to drying under a flow of air, the sheets were bombarded with argon plasma for 30 min to eliminate the native oxide layer on their surfaces. To augment the interfacial adhesion between the DLC film and the substrate, a CrN interlayer was deposited onto the interface of the substrates and DLC films. To examine the cross-sectional morphology of the DLC film, DLC films were deposited on Si wafers under the same deposition conditions as those utilized for coating the steel sheets.

2.2 Characterization

A field emission scanning electron microscope (FE-SEM; JSM-6701F, JEOL, Japan) was employed to examine the microscopic morphologies of the surfaces and wear tracks. The two-dimensional and three-dimensional morphologies of the wear tracks on the substrate were characterized via a white light interferometer (Bruker Contour GT, Germany). The surface morphology and roughness of the film were characterized using a noncontact atomic force microscope (AFM; FM-Nanoview 1000, China). A micro-Raman spectrometer (Jobin-Yvon HR-800, Horiba, France) was employed to investigate the bonding configurations of the DLC films. The states of C in the film and wear scars were characterized by X-ray photoelectron spectroscopy (XPS; Escalab 250 Xi, USA). To avoid interference, the sample surface was presputtered with a thin gold layer, and Au

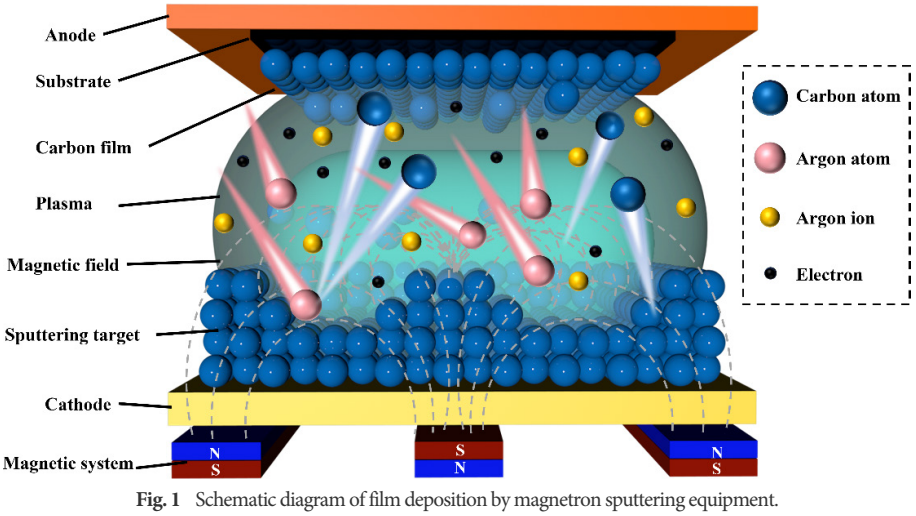

Fig. 1 Schematic diagram of film deposition by magnetron sputtering equipment.

was used for calibration during testing. A high-resolution transmission electron microscope (HRTEM; FEI Tecnai G2 F30, USA) was employed to characterize the nanostructures of the wear scars, with the samples prepared through focused ion beam (FIB) cutting technology. A Hysitron triboindenter (TI950, USA) was employed for the mechanical property characterization via nanoindentation, utilizing a Berkovich diamond tip. To eliminate the substrate effect on the measurement results, the indentation depth was stringently constrained to within less than 10% of the film thickness.

2.3 Fretting tests

The fretting friction testing equipment used in this study was independently developed and manufactured by Southwest Jiaotong University, and the relevant sensors were calibrated by the National Institute of Measurement and Testing Technology (China). This tangential fretting friction and wear testing machine employs a force closed-loop control strategy to achieve "soft landing"-type servo loading and dynamic force compensation loading. In this experiment, the loading module adopted a ball-on-disk contact mode, and the test environment was constant-temperature (25 °C) and constant-humidity (50% RH) atmospheric environment. DLC-deposited AISI 304 sheets and 100Cr6 steel balls were used as the substrate (lower specimen) and upper specimen, respectively. In the fretting experiment, the normal load was 1–10 N; the displacement amplitude was 1–10 μm; the frequency was 3 Hz; one set of experiments consisted of 3,600 cycles. The experimental parameters were selected through preliminary experiments and Hertzian calculations to ensure that they fell within the tolerable range of the DLC film. It is worth clarifying that the displacement amplitude discussed herein denotes the preset input parameter of the fretting friction testing machine, which represents the distance from the central position to the maximum unilateral displacement of the counter ball. Therefore, the distance moved in a complete operating cycle is four times the preset displacement amplitude.

3 Results and discussion

3.1 Characterization of DLC films

The basic information of the prepared DLC film is shown in Fig. 2. The cross-section of a newly cut sample, observed via SEM, reveals that the DLC film has a thickness of 2.507 μm, while the transition layer has a thickness of 1.536 μm (Fig. 2(a)). AFM was adopted for evaluating the microstructural characteristics of the DLC film surface, revealing an arithmetic mean roughness (R_a) of 6.89 nm (Fig. 2(b)). The DLC film's Raman spectrum is illustrated in Fig. 2(c). Following Gaussian fitting, two characteristic peaks are identified: the D peak centered at approximately 1,360 cm^{-1} and the G peak at approximately 1,580 cm^{-1}, with an intensity ratio (I_D/I_G) of 0.717. A broad asymmetric peak near 1,500 cm^{-1} is common in the Raman spectrum of DLC films. This broad peak can be decomposed and fitted into two peaks using Lorentzian or Gaussian functions, corresponding to the D peak and G peak, respectively. The D peak originates from the breathing vibrations of defects or aromatic rings in sp^2 sites, while the G peak corresponds to the E_{2g} zone-center vibrational mode (optically allowed) of crystalline graphite, serving as an indicator of the presence of sp^2 C–C hybrid bonds [32, 33]. Although Raman spectroscopy is unable to provide quantitative insights into the sp^2 and sp^3 hybridized carbon species in the film, the I_D/I_G ratio serves to estimate the relative content of sp^3 hybrid bonds. Specifically, for hydrogenated amorphous carbon films, a lower I_D/I_G ratio corresponds to a higher sp^3 hybrid bond content [34]. In the XPS

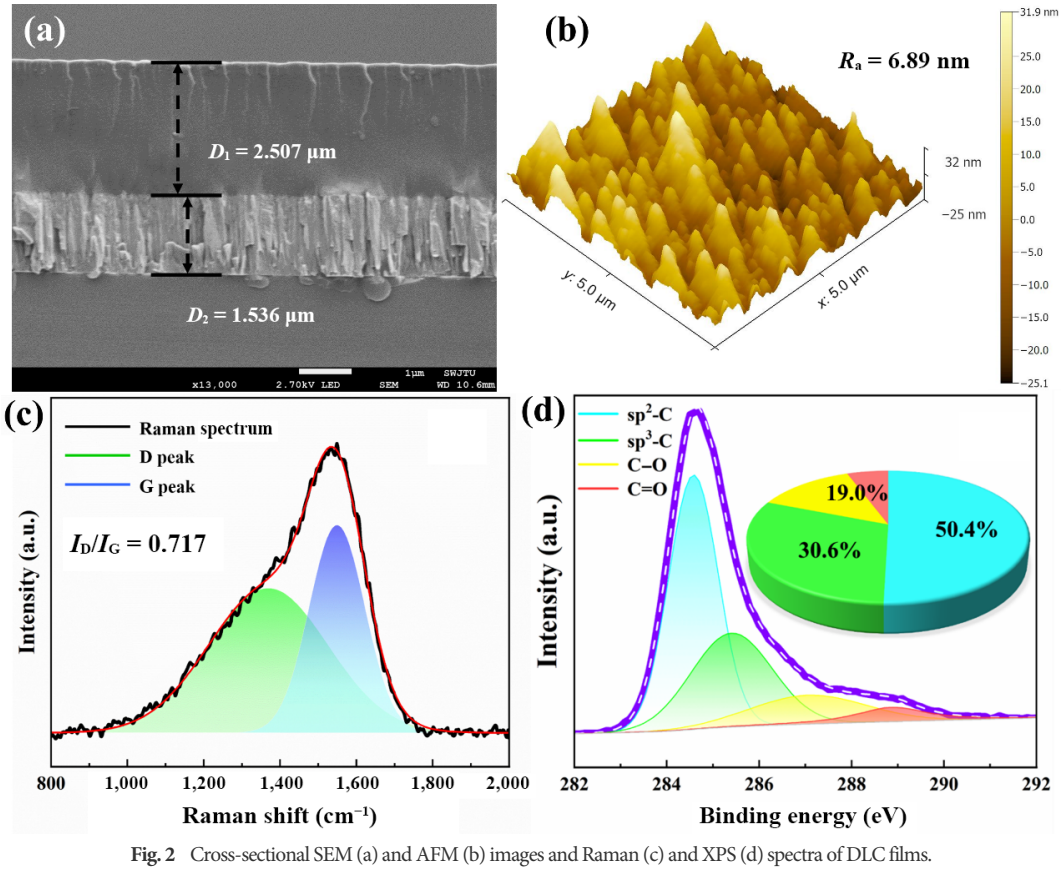

Fig. 2 Cross-sectional SEM (a) and AFM (b) images and Raman (c) and XPS (d) spectra of DLC films.

of DLC films, the main C 1s peak generally appears at approximately 285.1 eV, which is intermediate between diamond and graphite. Through Gaussian fitting, this peak can be decomposed into two characteristic peaks: a sp^2 peak centered at approximately 284.4 eV and a sp^3 peak at 285.2 eV. The relative ratio of sp^2 to sp^3 hybrid bonds is calculated from the area ratio of these two peaks, while the peaks at 287.1 and 288.9 eV (high binding energy region) are assigned to C–O or C=O chemical bonds. Therefore, Raman spectra and XPS are typically used in combination for the structural characterization of DLC films. Figure 2(d) presents the XPS spectrum of the prepared DLC film and the results of peak deconvolution. As depicted in the pie chart of the figure, the area ratios of the deconvoluted peaks correspond to 50.4% for sp^2 hybrid bonds, 30.6% for sp^3 hybrid bonds, and 19% for carbon–oxygen bonds (C–O and C=O). The nanohardness and elastic modulus of the DLC film, determined by nanoindentation, are 24.5 and 217 GPa, respectively, which are significantly higher than the substrate's respective values of 7.2 GPa (nanohardness) and 200 GPa (elastic modulus).

3.2 Fretting tribological properties

Fretting experiments were conducted using ball-on-disk contact modules (conforming to Mindlin's theory of elastic contact [35]) under different normal loads and displacement amplitudes to investigate the influences of operating conditions on the fretting behavior and regime of the DLC films. The friction force–displacement (Ft–D) curves, as the most fundamental and critical information in fretting friction, serve to analyze fretting operating states and provide a wealth of key parameters. Figure 3 depicts the tangential fretting Ft–D curves of the prepared DLC films under various normal loads and displacement amplitudes. Each set of curves provides two perspectives, clearly demonstrating the fretting operation states of the fretting pair at the corresponding displacement amplitudes and normal loads. Each complete fretting cycle is presented as a closed curve in the images. The Ft–D curves in the figure exhibit a characteristic parallelogram shape under the majority of working conditions, suggesting that the fretting regime is in the slip regime (SR) under these corresponding conditions. Notably, the curves under the working conditions of "5 N–1 μm", "7 N–1 μm", "9 N–1 μm", and "9 N–3 μm" show an approximately elliptical shape with pointed ends. As opposed to the parallelogram-shaped curves under other conditions, these curves are devoid of linear segments representing tangential displacement along the horizontal axis. Serving as a hallmark of PSR, this characteristic confirms the absence of gross relative slip between the two contact interfaces. The contact center remains in an adhesive state, where the tangential force is regulated through elastic deformation, while microslip occurs at the contact edges.

To depict the evolution of fretting states from partial slip to gross slip, Fouvry et al. [36] introduced three sets of parameter ratios (energy ratio, sliding ratio, and system-independent ratio) associated with Ft–D curves, enabling quantitative characterization of the fretting regime of friction pairs under given operational conditions. The energy ratio e, defined as the ratio of dissipated energy E_d to total system energy E_t per fretting cycle, is utilized in this study to quantitatively characterize the fretting regime of the friction pairs under test. As reported by Fouvry et al., $e = 0.2$ serves as the critical value delineating the transition from partial slip to gross slip. Consequently, a value of $e < 0.2$ indicates partial slip, whereas $e > 0.2$ corresponds to gross slip. Figure 4 depicts the E_d/E_t energy ratio curves of the DLC films under different normal loads and displacement amplitudes. The energy ratios remain below 0.2 only under the working conditions of "5 N–1 μm", "7 N–1 μm", "9 N–1 μm", and "9 N–3 μm", while those under other conditions are all greater than 0.2. For the majority of operating conditions, the Ft–D curves illustrated in the figure are characterized by a parallelogram shape, which demonstrates that the fretting regime falls within SR under the corresponding operating parameters.

While a multitude of factors affect the fretting regime, displacement amplitude and normal load are typically regarded as the two critical controllable parameters that dominate in most scenarios. With the normal load plotted on the vertical axis and the displacement amplitude on the horizontal axis, combining the fretting regime corresponding to different load–amplitude combinations enables the generation of an intuitive fretting regime distribution map that reflects the dependence on operating conditions. Such a diagram is generally referred to as the RCFM [14]. With a fixed friction pair, altering the operating conditions combined with the RCFM enables the regulation of fretting regimes. The RCFM of the DLC films presented in Fig. 5 was plotted by summarizing the Ft–D curves obtained under different operating conditions. It is noteworthy that no mix regime was observed in the fretting experiments of DLC films. The mix regime refers to the following process: After a period of fretting, work hardening and surface layer microstructural transformation occur on the material surface, leading to a significant increase in friction force. The Ft–D curve becomes increasingly closed and even linear. At this stage, the contact center maintains an adhesive state, and the fretting regime undergoes a transition from gross slip to partial slip. Following a period of operation in PSR, the contact state switches from the adhesive state back to the slip state, coupled with an abrupt reduction in friction force. After further operation for a period, work hardening (i.e., microstructure transformation) occurs again at the contact interface, and this cycle repeats. In this process, significant damage will be caused to the substrate material.

In addition to identifying the existing fretting regime, the Ft–D curves can also provide additional critical insights into the fretting behavior. The curve corresponding to the gross slip (Fig. 6(a)), when observed from a perspective perpendicular to the friction force–displacement amplitude plane, exhibits three distinct stages [27]: sticking phases (①–②, ④–⑤), microslip phases (②–③, ⑤–⑥), and gross slip phases (③–④, ⑥–①). Entirely derived from the elastic deformation of contact interface asperities, the sticking regime results in a linear relationship between the friction force and relative displacement at this stage. This correlation may be described using the average tangential stiffness, with the slope of the adhesion stage representing the substrate's average tangential stiffness. Subsequently, as the friction force increases, relative slip starts to occur at some contacting asperities, while the remaining parts stay in a sticking state, with microslip initiating at this stage. The gross slip state is reached when all contacting asperities begin to undergo relative slip. In brief, the average slope of the ①–③ curve segment is able to characterize the inherent average slip stiffness belonging to the substrate material, with the area bounded by the closed curve enabling quantification of the energy dissipated within a full fretting cycle [10].

With an increase in displacement amplitude, the friction coefficient exhibits an upward trend (Fig. 6(b)). This can be ascribed to the larger displacement amplitude inducing the fretting regime to transition from partial slip to gross slip. For a given friction system, the central region of partial slip is in a sticking state (static friction), with microslip restricted solely to the margins of the contact zone; consequently, a lower friction

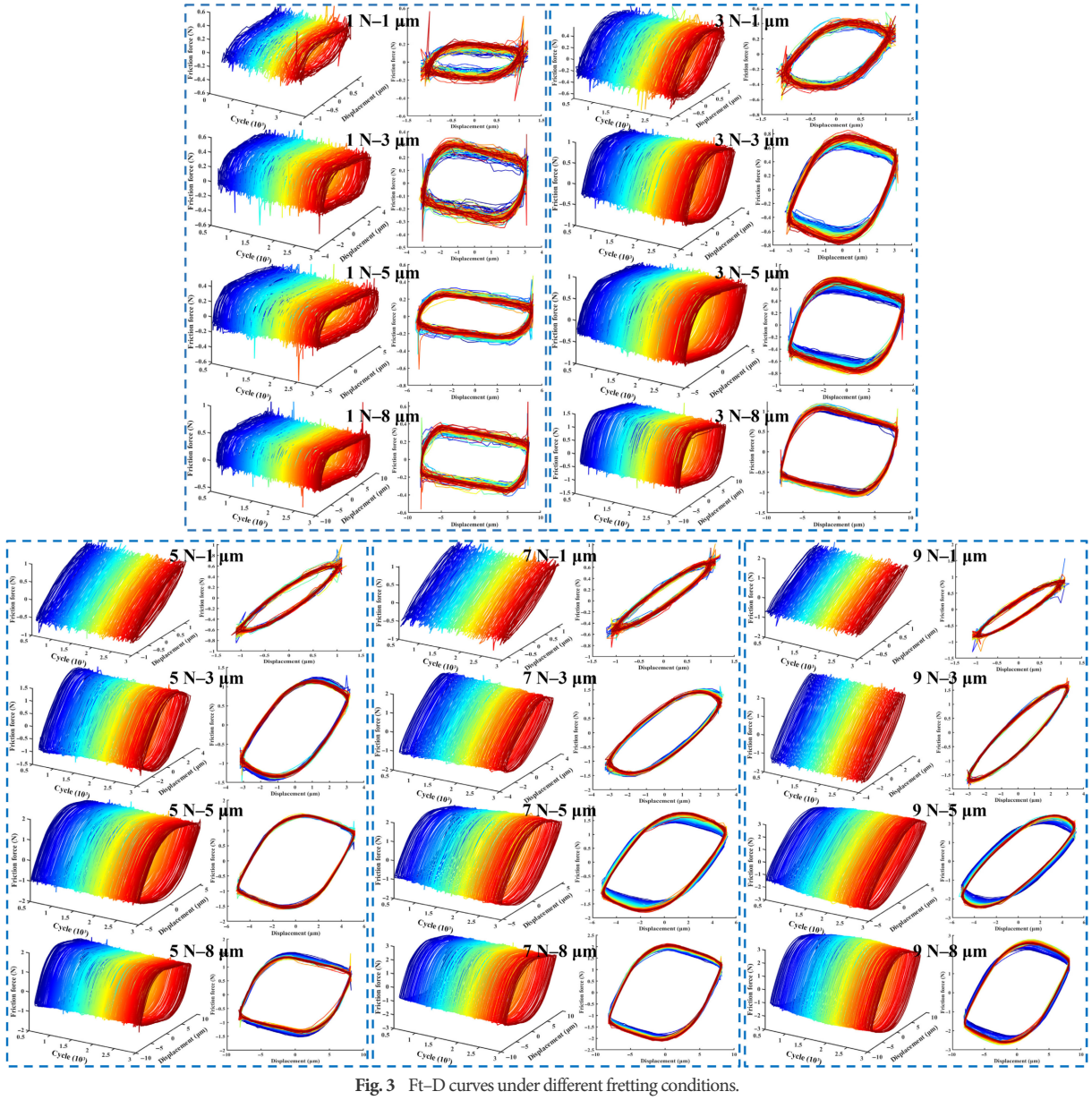

Fig. 3 Ft–D curves under different fretting conditions.

coefficient is generated compared to that in SR. Under a fixed displacement amplitude, the friction coefficient displays an inverse tendency with the elevation of the normal load, which is in agreement with the properties of sliding friction [37]. The normal load exerts its influence on the friction coefficient predominantly through its effect on the actual contact area. Typically, the friction coefficient bears a proportional relationship to the ratio of the actual contact area to the normal load [38]. Calculations based on Hertzian contact theory [39] demonstrate that the rate of growth of the contact interface upon load elevation is slower than the rate at which the load increases. Consequently, the friction coefficient exhibits a reduction with the elevation of the load.

During fretting experiments, the displacement amplitudes and normal loads are typically small, leading to a modest amount of generated wear and thus a high probability of inaccuracies in wear volume determination with a 3D profilometer. However, the wear volume produced in fretting tests has been found to have a linear relationship with the accumulated dissipated energy [40]. Therefore, to ensure data accuracy, this paper quantitatively compares the wear volumes under different operating conditions by comparing the dissipated energy. Figure 6(c) shows the average dissipated energy under different fretting conditions. As seen from the figure, increases in both displacement amplitudes and normal loads lead to an increase in dissipated energy. Moreover, when the normal load steadily grows, the influence of changes in displacement amplitude on dissipated energy becomes more significant. This is attributed to the fact that a greater normal load enhances the tangential force, whereas an increased displacement amplitude intensifies the relative displacement; thus, the dissipated energy and wear volume will inevitably increase. Figure 6(d) shows the variation law of the tangential stiffness with the normal load and displacement amplitude. Tangential stiffness is also of great significance in the fretting state. A decrease in tangential stiffness indicates an increase in elastic deformation of the contact interface, which in turn leads to a decrease in the relative slip amplitude. The tangential stiffness rises with increasing normal load but declines with increasing displacement amplitude.

3.3 Exploration of the lubrication mechanism

With the aim of investigating the wear mechanisms of DLC films under different fretting regimes, SEM was used to capture images

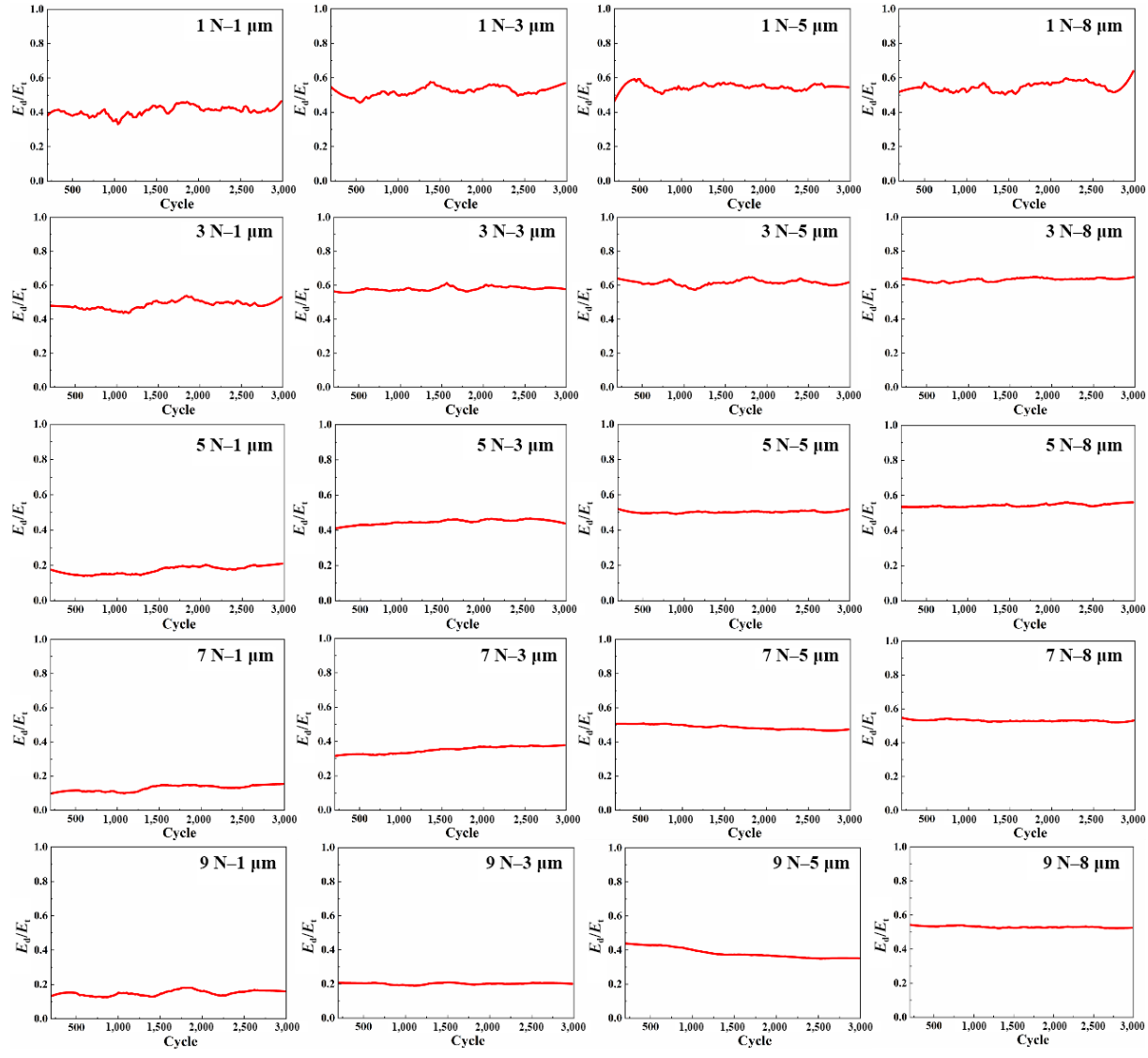

Fig. 4 Energy ratio curves.

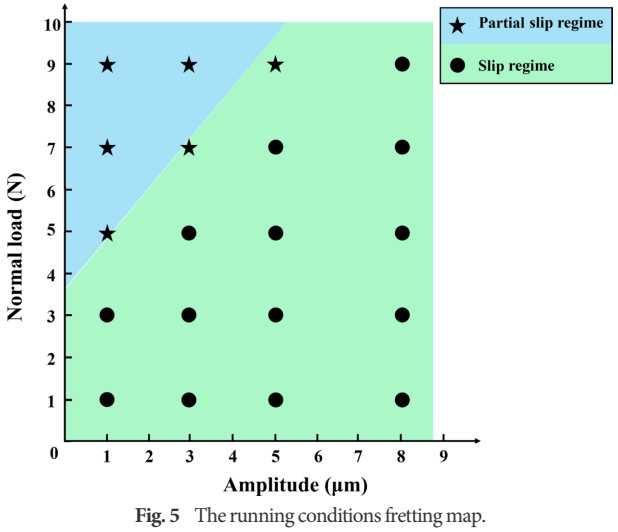

Fig. 5 The running conditions fretting map.

of wear scar (on the counterpart ball) morphologies in PSR (10 N–2 μm) and SR (10 N–10 μm), which are displayed in Figs. 7 and 8. Figure 7(a) presents the general view of the wear scar under PSR. White wear debris is mainly concentrated at the wear scar's perimeter, enabling identification of the scar's approximate range. Overall, the wear behavior in partial slip is comparatively slight, with the entire wear scar being circular and no obvious damage marks. Under higher magnification, Fig. 7(b) illustrates the image of the wear scar edge, while Fig. 7(c) shows that of the wear scar center. It can be seen that there are no obvious wear scar tracks at the wear scar edge except for wear debris. In the contact center area, some spot-like protrusions and striations can be observed. Therefore, this indicates that neither wear debris nor obvious wear scar tracks are generated in the contact center area. Figure 7(d) depicts the morphology of relatively large wear debris observed using SEM, which appears as agglomerated floccules and likely results from the friction between oxides on the film surface and the counterpart ball. Through comprehensive analysis of the wear scar morphology of DLC films in PSR, this finding aligns with the characteristic behavior of the fretting PSR in ball-on-plane contact [35]. Specifically, adhesion dominates the contact center, whereas microslip occurs at the contact periphery.

Figure 8(a) illustrates the wear scar in the gross slip, which is predominantly elliptical in shape, featuring distinct damage traces at its center and a substantial accumulation of wear debris at the periphery. As revealed by the higher-magnification micrographs (Fig. 8(b)), a multitude of plow-groove-shaped damage

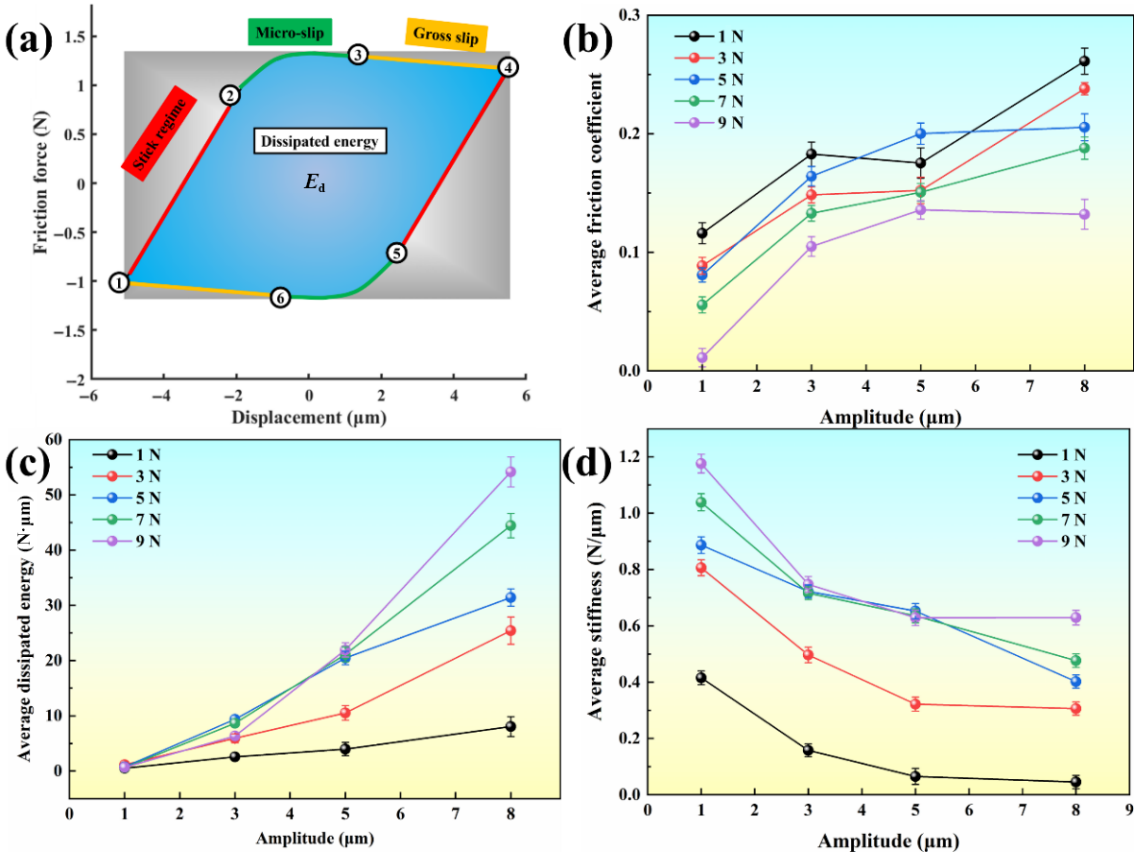

Fig. 6 Analysis of Ft–D curve (a), average friction coefficient curves (b), average dissipated energy curves (c), and average tangential stiffness curves (d) under different fretting conditions.

characteristics are present at the contact center of the wear scar, which suggests that relative displacement induces plastic deformation of the surface material, while the produced wear debris gives rise to substantial abrasive wear on the surface. Figure 8(c) presents a substantial wear debris particle at the wear scar periphery, along with the energy dispersive X-ray spectroscopy (EDS) area-scan elemental analysis results of this debris. This piece of wear debris is dominated by Fe and O, indicating that its main components are iron and iron oxides. This indicates that after the counterpart ball underwent fretting fatigue wear, work hardening occurred on its surface, and subsequently, the surface spalled due to embrittlement. Subsequently, the granular abrasive particles at the peripheral area of the wear scar underwent analysis (Fig. 8(d)). It was found that, except for some small wear debris particles that contain no iron, most granular wear debris contains C, O, and Fe, indicating that the wear debris is mainly mixtures of iron and carbon as well as their oxides.

From the Ft–D curves and friction coefficient curves, it is known that the DLC film did not fail in SR, and there was no direct contact between the AISI 304 stainless steel substrate and the 100Cr6 counterpart ball. Therefore, it can be judged that the Fe in the wear debris originated from the counterpart ball, which indirectly indicates that the DLC film has a considerable effect in enhancing the fretting wear resistance of the substrate. Empirically, although no obvious adhesive wear characteristics have been observed in the gross slip, a small amount of adhesive wear may still occur at the initial stage of the running-in period, which subsequently disappears with the formation of the third-body layer. An increase in displacement amplitude prolongs the contact duration of wear debris with air and enhances the likelihood of wear debris being oxidized [41].

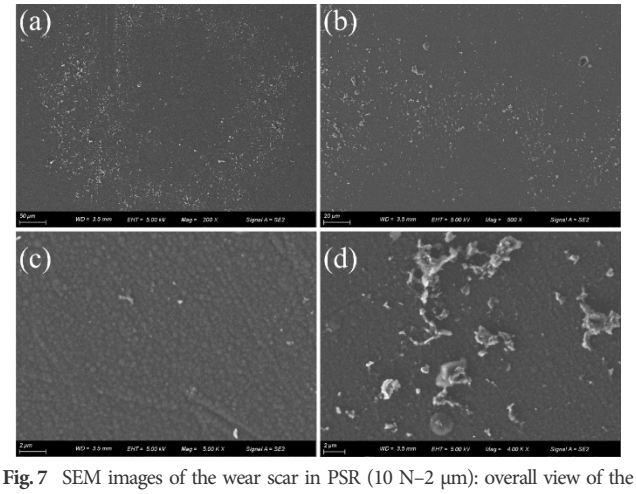

Fig. 7 SEM images of the wear scar in PSR (10 N–2 μm): overall view of the wear scar (a), edge of the wear scar (b), contact center of the wear scar (c), and wear debris (d).

Furthermore, cross-sections of the wear scars on the surface of the friction ball were produced via FIB (Fig. 9(a)). TEM images of these cross-sections were then captured. As shown in Fig. 9(b), the bottom layer corresponds to the 100Cr6 counterpart ball; the top layer is the protective layer prepared during FIB sampling, and the middle layer is a transfer film with a thickness of 0.17 μm. As observed in Fig. 9(c), a large number of ordered cluster structures are present in the transfer film, which contain iron, oxygen, and carbon elements, with relatively more iron and oxygen. Combined with the HRTEM images and selected area electron diffraction (SAED) pattern (Figs. 9(d) and 9(e)), which correspond to the

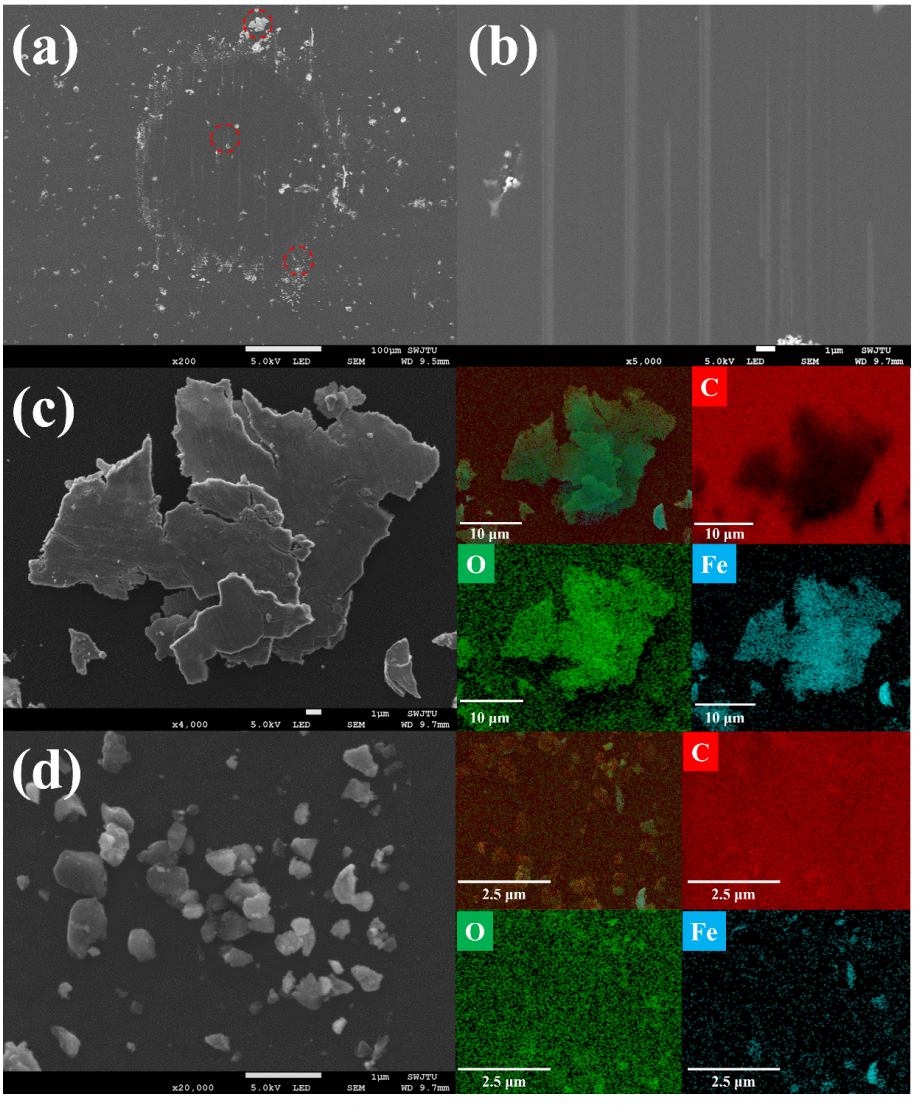

Fig. 8 SEM images of the wear scar in SR (10 N–10 μm): overall view of the wear scar (a), contact center of the wear scar (b), a substantial wear debris particle (c), and wear debris (d).

(110) crystal plane of body-centered cubic (bcc) iron (α-Fe) (with a lattice constant of approximately 2.866 Å), this confirms that the numerous ordered clusters in the transfer film are iron and iron oxides. The transfer film consists of amorphous carbon interspersed with crystalline iron oxides, forming a unique amorphous–nanocrystalline composite structure. The nanocrystalline iron oxides not only reduce the brittleness of the amorphous carbon film but also enhance its load-bearing capacity, while the encapsulation of iron oxides by the carbon film reduces the friction coefficient and alleviates abrasive wear to a certain extent [42, 43]. Therefore, the transfer film with such a composite structure can provide excellent lubricating performance. Notably, tribological white layers generally contain minimal or no oxygen [44, 45], whereas the third body layer generated from wear debris contains substantial oxides upon final transfer to the counterpart ball's surface. It was observed that the transfer film in this experiment not only contains a large amount of oxygen but also contains carbon from the counterpart material. Therefore, it can be concluded that what is formed on the counterpart ball's surface is a tribological transfer film, rather than a tribological white layer formed by microstructural transformation of the counterpart ball's surface layer [46].

Raman spectroscopy can simply and nondestructively distinguish the chemical bonding and structural composition of carbon-based films. Raman spectroscopy enables nondestructive differentiation of chemical bonds and structural configurations in carbon materials. Via Gaussian fitting, the asymmetric characteristic peak of DLC films at 1,500 cm^{-1} can be deconvoluted into the D band and G band: The D band at approximately 1,360 cm^{-1} originates from the breathing vibrations of aromatic rings with defects at sp^2 hybridized sites, while the G band at 1,580 cm^{-1} arises from the stretching vibrations of aromatic rings or carbon chains at sp^2 hybridized sites and serves as a characteristic indicator of sp^2 C–C hybrid bonds [47, 48]. The I_D/I_G serves as a criterion for determining the relative content ratio of sp^2 hybridized bonds to sp^3 hybridized bonds in the material [34]. Thus, in amorphous carbon materials, an increase in the I_D/I_G value indicates an enhanced degree of ordering. Furthermore, the full width at half maximum (FWHM) can also serve as a criterion for evaluating the crystallinity of films: Highly ordered carbon-based materials generally exhibit a narrowing characteristic in their FWHM, while disordered amorphous carbon typically has broader FWHM values. Figure 10 compares the Raman spectral information of the contact surfaces of the friction pairs under the two fretting regimes. From Fig. 10(a), it is evident that along the progression from the substrate DLC film to

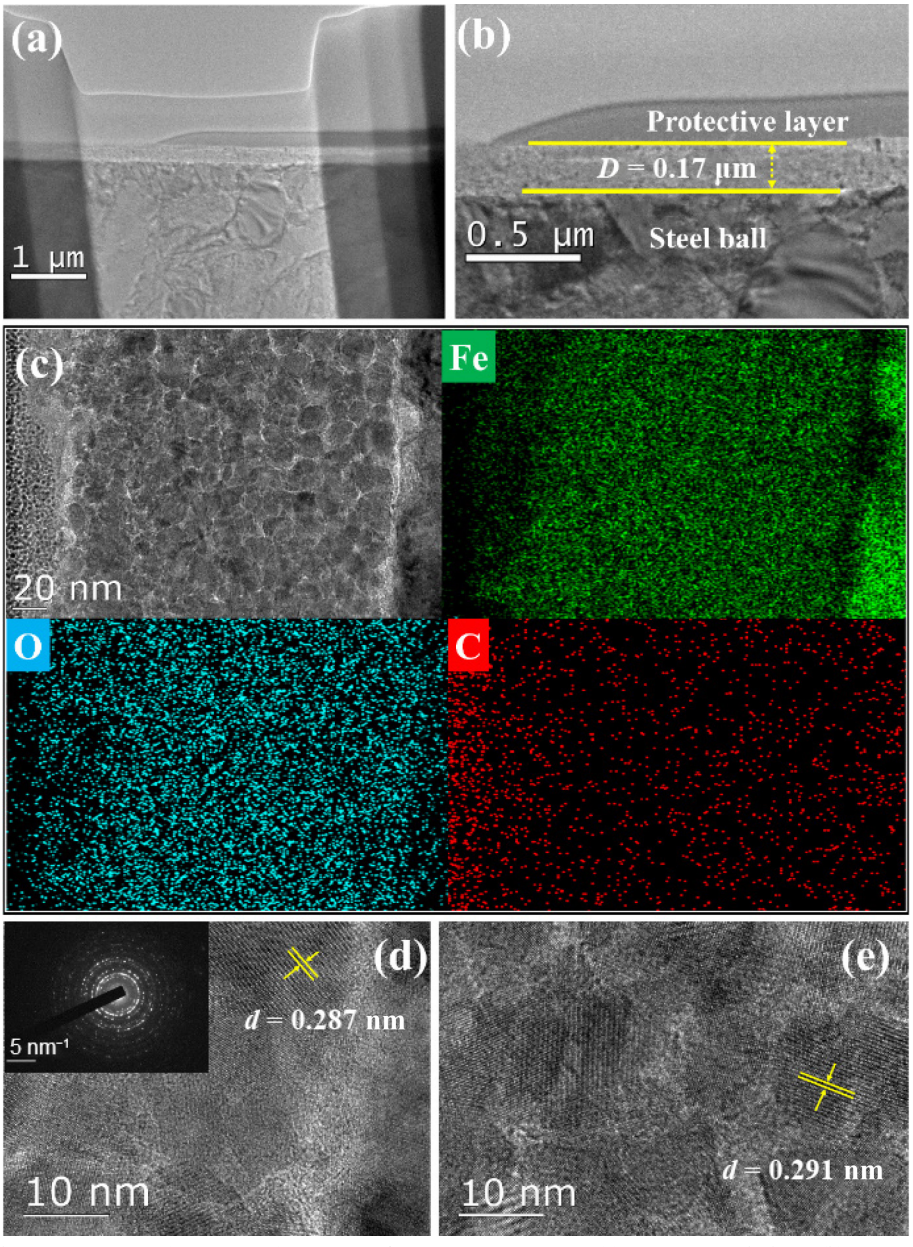

Fig. 9 TEM images of the wear scar in SR (10 N–10 μm): overview of wear scar cross-sections (a), cross-section thickness (b), TEM image and EDS mapping maps (c), and high-magnification TEM images (d, e).

the partial slip and subsequently to the gross slip, the D peak intensity exhibits a substantial increase, while the G peak undergoes a gradual shift toward higher wavenumbers. This result verifies a decrease in the extent of bond angle disorder among sp^2 hybrid bonds and a rise in the proportion of sp^2 hybrid bond configurations. Gaussian fitting was performed separately on the contact interfaces corresponding to the two fretting regimes (Figs. 10(c)–10(f)). Figure 10(b) presents the changes in I_D/I_G values and FWHM of the G peak for the substrate DLC film and under the two fretting regimes. It can be observed that after fretting, the I_D/I_G value increased while the FWHM decreased; compared with those at the wear tracks, the I_D/I_G values of the wear scars were higher and the FWHM was lower; additionally, at SR, the I_D/I_G value was higher and the FWHM was lower compared with those in PSR. These spectral variations collectively validate an elevated content of sp^2-hybridized carbon and improved structural ordering within the amorphous carbon matrix. In the context of carbon-based tribomaterials, such changes are direct evidence of a progressive enhancement in the graphitization degree [26, 49]. The more prominent I_D/I_G elevation and G peak narrowing in SR are attributed to the more intense interfacial shear stress and prolonged contact interaction, which facilitate the rearrangement of carbon atoms toward a more thermodynamically stable graphite-like structure.

To this point, the tangential fretting wear mechanisms and friction-reducing/anti-wear mechanisms of DLC films can be summarized as follows: In the PSR, the contact center remains adhesive, leading to very slight damage. Microslip takes place at the peripheral regions of the contact interface, generating only a minimal amount of wear debris and resulting in exceptionally low overall wear.

At the contact interface in the PSR, the DLC film undergoes a mild graphitization transition driven by interfacial shear and localized contact stress. A small fraction of wear debris, characterized by a higher graphitization degree relative to the bulk film, adheres to the friction ball's surface—serving as a nascent

lubricating medium that mitigates direct contact between the film and the counterpart. In contrast, within SR, the surface microasperities of the DLC film are subjected to the combined action of tangential shear stress and normal compressive stress. Under this composite loading, these microasperities undergo plastic deformation and subsequent detachment, ultimately generating abrasive particles. These particles not only participate in the three-body friction process but also contribute to the evolution of the contact interface by inducing plowing effects on the film surface. Thus, abrasive wear takes precedence as the dominant wear mechanism for the DLC film. Concurrently, the contact interface of the counterpart ball suffers fatigue wear, which is induced by cyclic reciprocating sliding that generates alternating stress on the surface. Furthermore, with the increase in displacement amplitude, the interaction duration between the wear interface, wear debris, and ambient air is extended—this prolonged exposure facilitates the diffusion of oxygen to the contact region, ultimately triggering oxidative wear on the interface.

The wear debris mainly consists of iron-carbon mixtures and their oxides. With the progression of fretting, the carbon in the wear debris gradually graphitizes and mixes with iron oxides formed from iron debris detached from the counterpart ball, forming the third-body layer that transfers to the friction ball surface. This forms a transfer film composed of a highly graphitized carbon film encapsulating iron oxides, which can further protect the substrate.

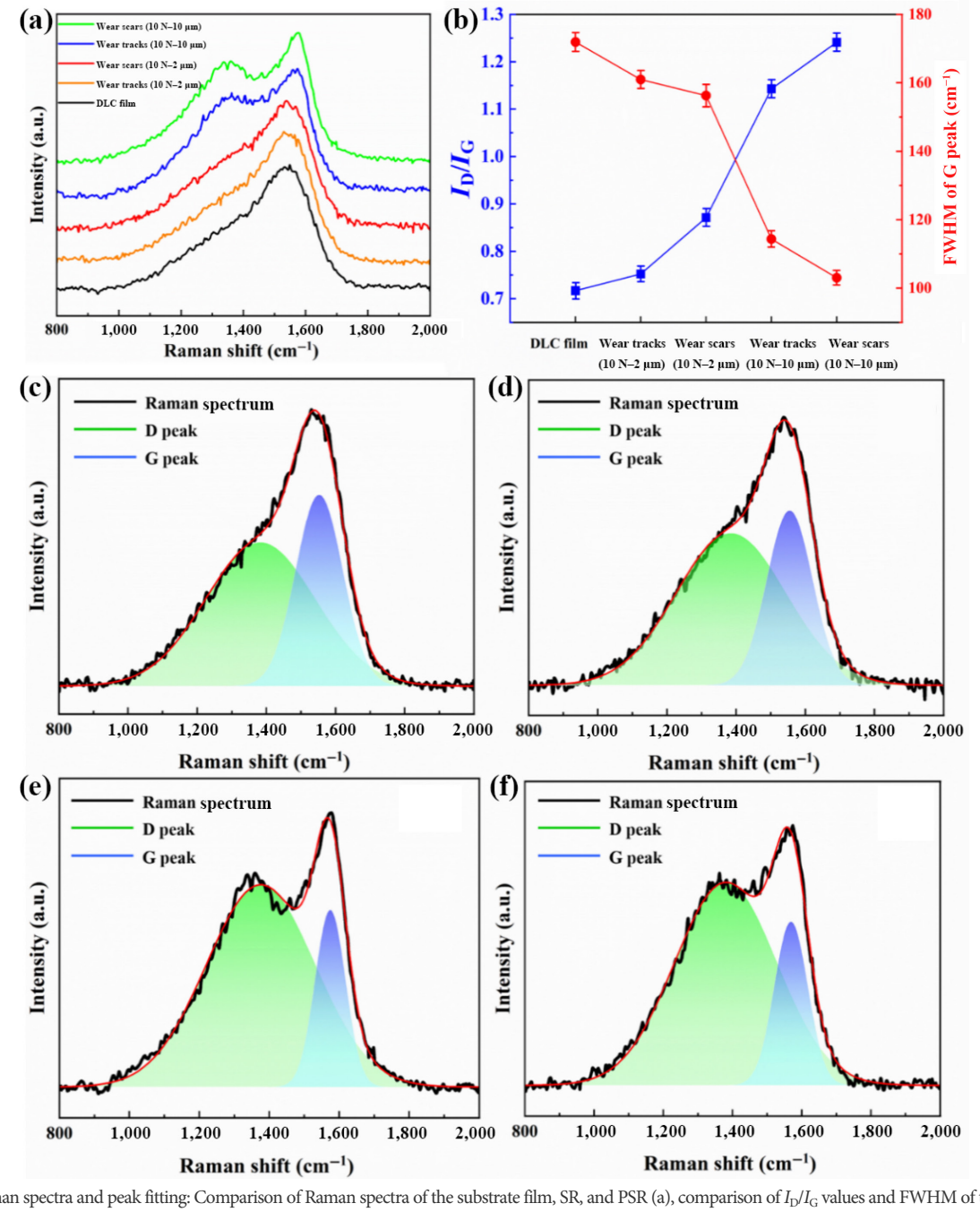

Fig. 10 Raman spectra and peak fitting: Comparison of Raman spectra of the substrate film, SR, and PSR (a), comparison of I_D/I_G values and FWHM of the G peak (b), Raman spectra and peak fitting of the wear track in PSR (c), wear scar in PSR (d), wear track in SR (e), and wear scar in SR (f).

4 Conclusions

This study systematically assessed the tangential fretting behavior of DLC films across various fretting conditions. The protective efficacy of DLC films on the substrate was verified, and an RCFM tailored to these films was constructed. Additionally, the influences of fretting conditions on fretting regime transitions and associated tribological properties were summarized, alongside the wear mechanisms and friction-reducing/anti-wear mechanisms of DLC films under both PSR and SR. The key conclusions are as follows:

(1) DLC films provide robust anti-wear protection for the substrate in both the PSR and SR of fretting. Under identical contact conditions, the friction coefficient and wear volume in PSR are substantially lower than those observed in the gross slip—attributed to the limited relative displacement and dominant elastic deformation at the contact interface in the partial slip state.

(2) An increase in normal load drives the fretting regime to transition toward PSR, accompanied by a progressive reduction in the friction coefficient and simultaneous increases in wear volume, dissipated energy, and tangential stiffness. In contrast, elevated displacement amplitude promotes the evolution of the fretting regime toward SR, resulting in a higher friction coefficient, increased wear volume and dissipated energy, as well as a gradual decline in tangential stiffness. This trend arises from the enhanced interfacial shear and relative sliding induced by larger displacement amplitudes.

(3) Within SR, during the running-in stage of DLC films, microasperities at the contact interface generate wear debris under the combined action of tangential force and compressive stress. This debris aggregates to form a third-body layer, which ultimately transfers to the counterpart ball. This transfer process leads to the formation of a tribological transfer film with a distinct amorphous–nanocrystalline composite structure—comprising graphitized carbon as a matrix encapsulating iron oxide particles (derived from the counterpart ball). This transfer film acts as a lubricating and protective barrier, effectively reducing the friction coefficient and mitigating fretting wear of the substrate.

Acknowledgements

The authors gratefully acknowledge the financial support provided by the National Natural Science Foundation of China (No. U2141211), the Postdoctoral Fellowship Program of the China Postdoctoral Science Foundation (No. GZB20250226), and the Innovation Project of Southwestern Institute of Physics (No. 202301XWCX003).

Declaration of competing interest

The authors have no competing interests to declare that are relevant to the content of this article. The authors Minhao Zhu and Junyan Zhang are the Editorial Board members of this journal.

References

[1] Szolwinski M P, Farris T N. Mechanics of fretting fatigue crack formation. *Wear* **198**(1–2): 93–107 (1996)

[2] Wang S J, Yue T Y, Wang D G, Abdel Wahab M. Effect of wear debris on fretting fatigue crack initiation. *Friction* **10**(6): 927–943 (2022)

[3] McCarthy O J, McGarry J P, Leen S B. Micro-mechanical modelling of fretting fatigue crack initiation and wear in Ti–6Al–4V. *Int J Fatigue* **62**: 180–193 (2014)

[4] Zhang T F, Su J, Ke L L. Fretting wear behavior of silicone rubber with biomimetic surface texture. *Friction* **13**(8): 9441000 (2025)

[5] Wang Q F, Wang H L, Wang Y X, Yan F Y. The influences of several carbon additions on the fretting wear behaviors of UHMWPE composites. *Tribol Int* **93**: 390–398 (2016)

[6] O'Halloran S M, Shipway P H, Connaire A D, Leen S B, Harte A M. A combined wear-fatigue design methodology for fretting in the pressure armour layer of flexible marine risers. *Tribol Int* **108**: 7–15 (2017)

[7] Ren Y P, Nie H L, Dong Y T, Xu X J, He J F, Li Z W, Cai Z B, Shen H M, Zhu M H. Fretting wear behavior of different surface modified layers of a tight fit spline used for a gauge-changeable railway vehicle. *Tribol Int* **193**: 109359 (2024)

[8] Zhu C F, He J F, Peng J F, Ren Y P, Lin X Z, Zhu M H. Failure mechanism analysis on railway wheel shaft of power locomotive. *Eng Fail Anal* **104**: 25–38 (2019)

[9] Wang H, Li H C, Zhao Y, Liu X T, Peng J F, He L P, Liu J H, Zhu M H. Fatigue failure mechanism of aluminium alloy riveted single-shear lap joints. *Eng Fail Anal* **146**: 107055 (2023)

[10] Gimpl V, Fantetti A, Klaassen S W B, Schwingshackl C W, Rixen D J. Contact stiffness of jointed interfaces: A comparison of dynamic substructuring techniques with frictional hysteresis measurements. *Mech Syst Signal Pr* **171**: 108896 (2022)

[11] Ding H H, Fridrici V, Geringer J, Fontaine J, Kapsa P. Low-friction study between diamond-like carbon coating and Ti–6Al–4V under fretting conditions. *Tribol Int* **135**: 368–388 (2019)

[12] Wang Z Y, Xiang Q R, Tan X, Zhang Y D, Zhu H Q, Pu J, Sun J K, Sun M L, Wang Y K, Wei Q, et al. Functionalized cortical bone-inspired composites adapt to the mechanical and biological properties of the edentulous area to resist fretting wear. *Adv Sci* **10** (11): 2207255 (2023)

[13] Zhang X G, Zhang Y L, Jin Z M. A review of the bio-tribology of medical devices. *Friction* **10**(1): 4–30 (2022)

[14] Zhu M H, Zhou Z R. On the mechanisms of various fretting wear modes. *Tribol Int* **44**(11): 1378–1388 (2011)

[15] Zhou Z R, Vincent L. Lubrication in fretting—A review. *Wear* **225–229**: 962–967 (1999)

[16] Zhang J, Wheatley A, Pasaribu R, Worthington E, Matthews S, Zinser C, Cann P. Wind turbine lubrication: Low temperature fretting wear behaviour of four commercial greases. *Tribol Int* **187**: 108706 (2023)

[17] Maruyama T, Saitoh T, Yokouchi A. Differences in mechanisms for fretting wear reduction between oil and grease lubrication. *Tribol T* **60**(3): 497–505 (2017)

[18] Zhou Z R, Liu Q Y, Zhu M H, Tanjala L, Kapsa P, Vincent L. An investigation of fretting behaviour of several metallic materials under grease lubrication. *Tribol Int* **33**(2): 69–74 (2000)

[19] Erdemir A, Eryilmaz O L, Fenske G. Synthesis of diamondlike carbon films with superlow friction and wear properties. *J Vac Sci Technol A* **18**(4): 1987–1992 (2000)

[20] Robertson J. Diamond-like amorphous carbon. *Mater Sci Eng R—Rep* **37**(4–6): 129–281 (2002)

[21] Sun L, Yang Z X, Zhang B, Xing Z Y, Zhang J Y, Wang F G, Qiang L. Superlubricity via *operando* formation of MoS_2/S_8 heterojunctions on steel surface with amorphous carbon protection. *Nano Energy* **123**: 109404 (2024)

[22] Kabir M S, Zhou Z F, Xie Z H, Munroe P. Designing multilayer diamond like carbon coatings for improved mechanical properties. *J Mater Sci Technol* **65**: 108–117 (2021)

[23] Han Z Y, Li H K, Lin G Q, Dong C. Influence of nitrogen flow rate on the microstructure and properties of N and Me (Me = Cr, Zr) co-doped diamond-like carbon films. *J Mater Sci Technol* **26**(11): 967–972 (2010)

[24] Sutton D C, Limbert G, Stewart D, Wood R J K. The friction of diamond-like carbon coatings in a water environment. *Friction* **1**(3): 210–221 (2013)

[25] Zhou Z R, Fayeulle S, Vincent L. Cracking behaviour of various aluminium alloys during fretting wear. *Wear* **155**(2): 317–330 (1992)

[26] Al-Azizi A A, Eryilmaz O, Erdemir A, Kim S H. Surface structure of

hydrogenated diamond-like carbon: Origin of run-in behavior prior to superlubricious interfacial shear. *Langmuir* **31**(5): 1711–1721 (2015)
[27] Yue Z F, Wang H, Fan X Q, Li H, Zhang J Y, Zhu M H. Regulating the fretting behavior of diamond-like carbon films by changing the composition and structure. *Carbon* **212**: 118097 (2023)
[28] Braceras I, Ibáñez I, Dominguez-Meister S, Velasco X, Brizuela M, Garmendia I. Electro-tribological properties of diamond like carbon coatings. *Friction* **8**(2): 451–461 (2020)
[29] Chen X C, Li J J. Superlubricity of carbon nanostructures. *Carbon* **158**: 1–23 (2020)
[30] Jang S, Chen Z, Kim S H. Origin of superlubricity of diamond-like carbon (DLC). *Friction* **13**(1): 9440995 (2025)
[31] Chen Q C, Xu X Y, Li A, Zhang Q D, Yang H M, Qiu N, Wang Y. Fretting wear resistance of amorphous/amorphous (AlCrFeNi)N/TiN high entropy nitride nanolaminates. *J Mater Sci Technol* **182**: 41–53 (2024)
[32] Erdemir A, Donnet C. Tribology of diamond-like carbon films: Recent progress and future prospects. *J Phys D Appl Phys* **39**(18): R311 (2006)
[33] Schall J D, Gao G T, Harrison J A. Effects of adhesion and transfer film formation on the tribology of self-mated DLC contacts. *J Phys Chem C* **114**(12): 5321–5330 (2010)
[34] Ferrari A C, Robertson J. Interpretation of Raman spectra of disordered and amorphous carbon. *Phys Rev B* **61**(20): 14095–14107 (2000)
[35] Mindlin R D. Compliance of elastic bodies in contact. *J Appl Mech* **16**(3): 259–268 (1949)
[36] Fouvry S, Kapsa P, Vincent L. Analysis of sliding behaviour for fretting loadings: Determination of transition criteria. *Wear* **185**(1–2): 35–46 (1995)
[37] Yue Z F, Wang Y F, Zhang J Y. Microstructure changes of self-mated fullerene-like hydrogenated carbon films from low friction to super-low friction with the increasing normal load. *Diam Relat Mater* **88**: 276–281 (2018)
[38] Greenwood J A, Williamson J B P. Contact of nominally flat surfaces. *P Roy Soc A—Math Phy* **295**(1442): 300–319 (1966)
[39] Hoeppner D W, Gates F L. Fretting fatigue considerations in engineering design. *Wear* **70**(2): 155–164 (1981)
[40] Fouvry S, Kapsa P, Zahouani H, Vincent L. Wear analysis in fretting of hard coatings through a dissipated energy concept. *Wear* **203–204**: 393–403 (1997)
[41] Zhuang W H, Fan X Q, Li W, Li H, Zhang L, Peng J F, Cai Z B, Mo J L, Zhang G G, Zhu M H. Comparing space adaptability of diamond-like carbon and molybdenum disulfide films toward synergistic lubrication. *Carbon* **134**: 163–173 (2018)
[42] Kametani N, Nakamura M, Yashiro K, Takaki T. Molecular dynamics simulation of the residual stresses within diamond-like carbon films on iron substrates. *Diam Relat Mater* **151**: 111860 (2025)
[43] Zhu X H, Wang X W, Liu Y H, Luo Y Y, Zhang H, Li B, Mao D B. Effect of cuttings particle content on the tribological behavior of Fe/DLC at casing and drill pipe joints: A molecular dynamics study. *J Mol Liq* **396**: 124006 (2024)
[44] Wild E, Reimers W. Residual stress and microstructure in the rail/wheel contact zone of a worn railway wheel. *Mater Sci Forum* **524–525**: 911–916 (2006)
[45] Sauger E, Fouvry S, Ponsonnet L, Kapsa P, Martin J M, Vincent L. Tribologically transformed structure in fretting. *Wear* **245**(1–2): 39–52 (2000)
[46] Chen X, Han Z, Lu K. Wear mechanism transition dominated by subsurface recrystallization structure in Cu–Al alloys. *Wear* **320**: 41–50 (2014)
[47] Erdemir A, Eryilmaz O. Achieving superlubricity in DLC films by controlling bulk, surface, and tribochemistry. *Friction* **2**(2): 140–155 (2014)
[48] Ferrari A C, Robertson J. Raman spectroscopy of amorphous, nanostructured, diamond-like carbon, and nanodiamond. *Philos T Roy Soc A* **362**(1824): 2477–2512 (2004)
[49] Erdemir A. Genesis of superlow friction and wear in diamondlike carbon films. *Tribol Int* **37**(11–12): 1005–1012 (2004)

Zhaofan Yue received his Ph.D. degree in materials science and engineering from Southwest Jiaotong University in 2024. Currently, he is pursuing postdoctoral research at the Southwest Institute of Physics, China National Nuclear Corporation, with his main research focus on solid lubrication, fretting wear, and corrosion and protection of materials.

Xiaoqiang Fan received his bachelor degree in 2011 from Qingdao University of Science & Technology and his Ph.D. degree from Lanzhou Institute of Chemical Physics, Chinese Academy of Sciences in 2016. He is currently a professor at Southwest Jiaotong University. His research focuses on lubricating materials, corrosion protection, and engineering applications. He has published over 130 papers in international journals, which received more than 1,300 citations.

Fanya Jin received his bachelor degree in 2001 from Anhui University and Ph.D. degree from Southwest Institute of Physics, China National Nuclear Corporation in 2007. He currently holds the position of researcher at the Southwest Institute of Physics. His main research work focuses on plasma applications, material surface modification technologies, and the first wall of the ITER shielding blanket.

Minhao Zhu received his bachelor and master degrees from Southwest Jiaotong University in 1990 and 1993, respectively. Then, he worked at Southwest Jiaotong University. From 1996 to 2001, he pursued his Ph.D. degree from Southwest Jiaotong University. His current position is a professor and doctoral supervisor. His research areas cover fretting wear, fretting fatigue, surface engineering, and the design of fastener connections. He has published over 400 papers in international journals such as *Carbon*, *Tribology International*, *Surface & Coatings Technology*, *Tribology Letters*, *Wear*, and *Friction*, which received more than 1,000 citations.